

Predicting the suitability of aqueous solutions of deep eutectic solvents for preparation of co-continuous porous carbons via spinodal decomposition processes

E. Posada^a, N. Lopez-Salas^a, D. Carriazo^{a,b,c}, M.A. Munoz-Marquez^b, C.O. Ania^d, R.J. Jimenez-Rioboo^a, M.C. Gutierrez^a, M.L. Ferrer^{a,*}, F. del Monte^{a*}

a Materials Science Factory, Instituto de Ciencia de Materiales de Madrid-ICMM, Consejo Superior de Investigaciones Científicas-CSIC, Campus de Cantoblanco, 28049, Madrid, Spain; *b* CIC Energigune, Parque Tecnológico de Alava, 01510, Miñano, Spain; *c* Ikerbasque, Basque Foundation for Science, 48011, Bilbao, Spain; *d* Instituto Nacional del Carbon-INCAR, Consejo Superior de Investigaciones Científicas-CSIC, C/Francisco Pintado Fe 26, 33011, Oviedo, Asturias, Spain

* Address correspondence to mferrer@icmm.csic.es or delmonte@icmm.csic.es

Keywords: Eutectic solvents, spinodal decomposition, porous carbons, Brillouin spectroscopy, NMR spectroscopy, aqueous binary mixtures.

Abstract

Spinodal decomposition (SD) processes have proved effective for the synthesis of macro- and mesoporous materials. Despite the theoretical aspects of SD processes are well understood, finding the proper experimental conditions – both the components as well as the ratio in which they have to be combined – to attain bicontinuous structures is a non-predictable and quite tedious process, typically based on trial and error. The challenge is therefore finding both a “tool” capable to predict the suitability of a particular starting solution to undergo a SD process. Here in, we have used aqueous solutions of DESs for the preparation of bicontinuous porous carbons via SD. Interestingly, morphologies range from spinodal- to aggregates-of-particle-like just depending on dilution. More interestingly, we also studied the starting DES/H₂O binary mixtures by Brillouin spectroscopy given the capability of this technique to observe local structure rearrangements resulting from non-ideal mixing. In our case, Brillouin spectra revealed the presence of a certain nanostructure in the macroscopically homogeneous DES/H₂O binary mixtures used for carbons preparation. Moreover, we also found that the representation of hypersonic velocity obtained from Brillouin spectroscopy revealed the occurrence of nanostructural rearrangements in a dilution range that coincided with that where carbons morphology transitioned from spinodal- to aggregates-of-particle-like. According to

these results, Brillouin spectroscopy allows predicting not only the suitability of a particular solution for the preparation of carbons via spinodal decomposition processes but also the range of dilutions for which this morphology will be ultimately obtained.

Introduction

Porous carbons are lately attracting considerable attention due to their potential in applications such as membranes for adsorption, filtration and separation,¹ catalytic supports,² electrodes in fuel cells, supercapacitors or batteries,^{3, 4, 5} or controlled release media,⁶ among others. In practical terms, hierarchical materials combining small and large pores are required. It is well known that the former are the main responsible of the activity – the larger the surface area, the higher the activity – but it is also worth noting that the ultimate performance of these materials is largely dependent on the accessibility to such an active surface. Thus, efforts must focus on the design of synthetic processes promoting the formation of bicontinuous structures of interconnected pores with mean diameters in the nano/micrometer range that allow mass transport throughout the whole monolithic structure.

A number of synthetic routes have been explored by using different carbonaceous precursors^{7, 8} and either hard or soft templates to modulate the porous texture of the resulting carbon structures.^{9, 10} In this regard, syntheses using hard-templates – where the pore structure is a replica of pre-synthesized mesoporous oxides and nanoparticles – typically suffer from a tedious procedure during the preparation and removal of templates – e.g. chemical etching. Thus, syntheses based on the use of soft-templates – via self-assembly of carbon precursors with block copolymers and surfactants that are sacrificed as porogens during carbonization – are considered as a more convenient approach. In this latter case, microphase separation induced by the well-ordered phases of self-assembled block copolymers and surfactants are responsible of the ultimate structure of the resulting materials. Nonetheless, the scale-up capability of these soft-template syntheses is questionable because the synthetic origin of most of block copolymers and surfactants make them costly and non-friendly in environmental terms.

Within this context, more environmentally benign and cost-effective phase separation processes have been investigated. Among others, spinodal decomposition (SD) processes have proved effective for the synthesis of macro- and mesoporous materials.^{11, 12, 13, 14, 15, 16} In this case, it is widely accepted that phase separations can be induced both thermally and chemically. Thermally induced phase separations are applied when the phase diagram of a certain polymer exhibits an upper critical solution temperature so that a homogeneous solution formed at a determined temperature is phase separated by thermal quenching. In chemically induced phase separations, the growth of oligomers/polymers makes them less and less soluble in the originally homogeneous starting solution and results in a phase-separation – i.e. between a polymer-rich and a polymer-depleted phase – that is ultimately frozen upon gelation when the growing polymers reach a certain degree of cross-linking. Diverse structures – e.g. interconnected or open-cell pores – can be

formed depending on the experimental parameters used for polymerization such as the solvent of choice and its volume fraction, and/or the temperature. Nonetheless, the transient structure that results from phase separation comes ultimately determined by the time relation between the onset of phase separation and gel formation – e.g. interconnected structures with a network-like morphology if the onset of both processes coincides, or with an aggregates-of-particles morphology if phase separation occurs earlier than gel formation so that the polymer-rich domains break-up and become spherical during the coarsening process of the SD in order to decrease the interfacial energy.^{17, 18, 19}

SD processes have been typically used for the preparation of porous metal oxides via sol-gel,^{17, 18, 20, 21, 22, 23, 24, 25, 26, 27, 28, 29, 30, 31} vinyl and acrylate polymers via radical polymerization,^{32, 33, 34, 35, 36, 37, 38, 39, 40, 41, 42, 43, 44} and epoxy, phenolic and furfuryl resins via condensation (Table 1).^{45, 46, 47, 48, 49, 50, 51, 52, 53, 54, 55, 56, 57, 58, 59, 60} It is worth noting that submission of some of these polymers – e.g. vinyl polymers as well as phenolic and furfuryl resins – to a carbonization process is a common process to obtain macroporous carbons.^{38-40, 50-60}

In practical terms, the achievement of bicontinuous structures via SD processes need of homogeneous starting solutions containing (1) the monomers/precursors that will form the final polymer/material and (2) a phase separation inducing agent – PSIA – that, at a certain stage of the process, segregate from the originally homogenous solution into a continuous phase. Eventually, the starting solution also contains (3) a co-solvent that helps to demix the phase separation inducing agent and the growing polymer into a bi-continuous-phase-separated system. The PSIA most widely used – either by its own or with the aid of some additional co-solvents – with every of the monomers/precursors has been polyethylene glycol (PEG) but the use of other polymers is also common – see, for instance, PO, PC, PDMS, or PAAM in Table 1. In these cases, both the polymer mass ratio – referred to the monomer/precursor – and the molecular weight have been used to control the SD process and thus obtain different morphologies. More recently, bicontinuous structures via SD processes have been obtained using different mass fractions of single co-solvents – e.g. formamide, ethylenglycol, ethanol, or even water in some few cases – as PSIAs (see Table 1). Despite the theoretical aspects of SD processes are well understood, finding the proper experimental conditions – both the components as well as the ratio in which they have to combine among – to attain bicontinuous structures via SD processes is a non-predictable and quite tedious process, typically based on trial and error. Thus, finding a “tool” capable to predict the suitability of a particular starting solution would indeed be challenging. For this purpose, we hypothesized that a simplification of the starting solutions by using single co-solvents as PSIAs – e.g. those described above or, at least, similar to – would be also of help to get the rationale behind the experimental aspects of the process.

Our group has recently reported on the preparation of bicontinuous porous carbons using deep eutectic solvents (DESs).^{61, 62, 63, 64, 65} DESs were first described by Abbot and coworkers in 2003⁶⁶ as supramolecular complexes formed between an hydrogen bond donor – HBD – and an hydrogen bond acceptor – HBA,

typically an ammonium or phosphonium salt. More recently, similar eutectics have also received the name of low-melting eutectic mixtures – by König and coworkers⁶⁷ – or low-transition-temperature mixtures – by Kroon and coworkers.⁶⁸ DESs share many characteristics with conventional ionic liquids (ILs) – e.g. non-reactive with water, non-volatile, and biodegradable – but the decrease in the melting point in DES is ascribed to the charge delocalization that occurs between the HDB and the HBA. In our case, DESs were composed of phenol derivatives and ammonium salts, so that the materials resulting after polycondensation exhibited a bicontinuous porous structure obtained via a SD process where the formation of a polymer-rich phase by polycondensation was accompanied by the segregation of the non-condensed matter – e.g. the ammonium salts – creating first a polymer-poor phase that, ultimately, becomes a polymer-depleted phase. We found that this phase-separation process ends with the formation of either interconnected or aggregates-of-particles-like structures but, despite we have been recently capable to tailor the textural properties of the resulting porous carbons,⁶⁹ we never rationalized the experimental conditions that let transitioning from one structure to another.

This paper contains two-well-separated parts. We first studied whether carbons prepared from DESs could exhibit different morphologies upon the control of the SD. The DES of choice was based on a mixture of resorcinol, glycerol, phosphoric acid and choline chloride in a 1:1:1:1 molar ratio. DES was studied by ¹H NMR spectroscopy and differential scanning calorimetry (DSC). This DES was used for the preparation of porous carbons via polycondensation with formaldehyde, and subsequent carbonization. As mentioned above, SD processes typically need of a PSIA that, at a certain stage of the process, segregate from the originally homogenous solution into a continuous phase. In our case, we just used water as co-solvent and different mass fractions of it – i.e. first, that originally coming from the formaldehyde solution and then, increasing this one upon further additions – to tailor the morphology of the resulting bicontinuous structure. The degree of condensation of the polymers resulting after polycondensation was studied by ¹³C-NMR and FTIR spectroscopies. The morphology of the resulting materials was studied by scanning and transmission electron microscopies. Further insights about the textural properties of the resulting carbons were obtained from N₂ and CO₂ adsorption/desorption isotherms, and Hg porosimetry. In the second part, we used Brillouin spectroscopy to study the starting DES/H₂O binary solutions aiming to find any physical insight that, in advance, may help to predict the suitability of these solutions in SD processes.

Experimental Section

Materials: Resorcinol (R), phosphoric acid (P), Glycerol (G), choline chloride (C) and formaldehyde (F, 37 wt% in aqueous solution) were purchased from Sigma-Aldrich and used as received. Water was distilled and deionized.

Preparation of carbons: The DES_{RPGC} was obtained by physical mixing of the individual components (R, P, G and C) and posterior thermal treatment at 90 °C overnight. The molar ratio among the components was 1:1:1:1. Phenolic resins were obtained from DES_{RPGC} following the procedure described in previous reports.⁶⁵ Briefly, F (37 wt% in aqueous solution) was added to DES_{RPGC} at a F to R molar ratio of 2:1. Afterwards, samples were thermally treated for 6 h at 60 °C and then for 4 days at 90 °C to become phenolic resins. The resin thus prepared was named as R_{RPGC80} where “80” indicates the DES mass fraction considering the sum of the mass of DES and water as 100%. R_{RPGC70}, R_{RPGC60}, R_{RPGC50}, R_{RPGC40}, R_{RPGC30}, and R_{RPGC20} were obtained upon the addition of the corresponding amount of water to every DES prior addition of F (see Table 2). After polycondensation, R_{RPGC} were submitted to a carbonization process – i.e. 800 °C for 4 hours in nitrogen atmosphere, with a heating ramp of 1.0 °C/min – to obtain the respective carbons – e.g. C_{RPGC80}, C_{RPGC70}, C_{RPGC60}, C_{RPGC50}, C_{RPGC40}, C_{RPGC30}, and C_{RPGC20}.

Sample characterization: DES_{RPGC} and its respective dilutions – e.g. DES_{RPGC80}, DES_{RPGC70}, DES_{RPGC60}, DES_{RPGC50}, DES_{RPGC40}, DES_{RPGC30}, and DES_{RPGC20}, see Table 1 – were studied by ¹H NMR spectroscopy using a Bruker spectrometer DRX-500. The samples were placed in capillary tubes, using deuterated water (D₂O) for dilution and deuterated chloroform (CDCl₃) as an external reference. DES_{RPGC} and its respective dilutions were also studied by high resolution Brillouin spectroscopy. Brillouin spectra were recorded using a Sandercock 3+3 Pass Fabry-Pérot interferometer⁷⁰ as Brillouin spectrometer and the light source was an Ar+ laser working at a wavelength (λ_0) of 514.5 nm. In this case, the liquid samples were placed in optical cuvettes (Starna) with 1 mm in optical path length. Experiments were performed using the 90A scattering geometry that is independent of the refractive index.⁷¹ The acoustic wave vector was $q^{90A} = [4 \pi \sin(\pi/4)] / \lambda_0$. The hypersonic sound propagation velocity (ν_H) was obtained from the relation between the Brillouin frequency shift (f) and q^{90A} , and expressed as $\nu_H = (2 \pi f) / q^{90A}$. Differential scanning calorimetry (DSC) was performed with a TA Instruments Model DSC Q-100 system, under a nitrogen atmosphere. The DSC scan was run in an aluminum pan in a sealed furnace, stabilized for 30 min at 50 °C, and then cooled to – 90 °C before heating at rates of 1 and 10 °C/min. Fourier transform infrared (FTIR) spectroscopy of R_{RPGC}-resins was performed in a FTIR spectrometer Bruker Model IFS60v. Solid-state ¹³C CPMAS NMR spectra of R_{RPGC}-resins were obtained using a Bruker Model AV- 400-WB spectrometer, by applying a standard cross-polarization pulse sequence. Elemental chemical analysis (ECA) of R_{RPGC}-resins was performed in an LECO Elemental Analyzer CHNS-932. Total Reflexion X-Ray Fluorescence (TXRF) analysis of R_{RPGC} resins was performed in a TXRF S2 PicoFox (Bruker), after a resins digestion in open vessel in nitric acid. The morphology of R_{RPGC}-resins and C_{RPGC}-carbons was studied via scanning electron microscopy (SEM), using a SEM Hitachi S-3000N system. N₂ adsorption/desorption isotherms were conducted using an ASAP 2010 from Micromeritics system on C_{RPGC}-carbons thermally treated overnight at 250 °C prior to nitrogen gas adsorption. Brunauer-Emmett-Teller (BET) theory and the Dubinin-Radushkevich method were used to calculate the specific surface areas (SBET)

and micropore volumes, respectively. CO₂ adsorption–desorption isotherms were performed at 0 and 25 °C in a Micromeritics Tristar 3020 instrument in the pressure range of 0.1-900 mbar.

Results and Discussion

Preparation of Porous Materials from DES/H₂O binary mixtures

As mentioned in the introduction, we first prepared the DES_{RPGC} composed of resorcinol (R), glycerol (G), phosphoric acid (P), and choline chloride (C) in a 1:1:1:1 molar ratio. This DES was obtained by simple thermal treatment at 90 °C of the physical mixture of the components. The formation of eutectic mixtures was first revealed by the liquid nature of the mixture at room temperature (Figure 1). Neither the melting (T_m) nor the crystallization temperatures (T_c) were clearly displayed in the DSC trace of the DES_{RPGC} (Figure 2), a common feature observed for non-easily crystallizable ILs and DESs.⁷² The formation of H-bond complexes was also confirmed by ¹H NMR spectroscopy – i.e. see the upfield chemical shift of the signals ascribed to R, G and C in DES_{RPGC} as compared to the chemical shifts of the individual components (see Figure S1 and Table S1 at Supporting Information).^{73, 74, 75, 76}

Polycondensation was promoted by addition of F to DES_{RPGC} with a fixed F to R molar ratio of 2 (Table 2). As described above, we prepared a set of samples upon addition of different amounts of water – e.g. R_{RPGC80}, R_{RPGC70}, R_{RPGC60}, R_{RPGC50}, R_{RPGC40}, R_{RPGC30}, and R_{RPGC20}. R_{RPGC80} was the sample with the minimum water content, coming from the aqueous F solution supplied by Sigma-Aldrich that we used for polycondensation. R_{RPGC70}, R_{RPGC60}, R_{RPGC50}, R_{RPGC40}, R_{RPGC30}, and R_{RPGC20} samples were obtained upon addition of further water fractions to the aqueous F solution (Table 2). Condensation between R and F was assessed by FTIR and solid-state ¹³C CPMAS NMR spectroscopies. The FTIR spectra of every resin revealed the presence of bands ascribed to methylene (C–H stretching and bending modes at ca. 2953 and 1475 cm⁻¹, respectively) and to methylene oxide groups (C–O benzyl ether groups at about 1091 and 1220 cm⁻¹), both indicative of a significant number of linkages between R rings (Figure S2).⁷⁷ The ν_3 and ν_1 modes of phosphoric acid typically produce bands at 1183, 1003, and 882 cm⁻¹ so their appearance in the spectra indicated the presence of phosphoric acid entrapped into the phenolic resin.⁶⁵ Solid-state ¹³C CPMAS NMR spectroscopy provided further insights with regard to the polycondensation issue (Figure S3). The signal at 151 ppm corresponded to aromatic phenolic carbons and its intensity could be used as an internal reference to estimate the polycondensation degree. Polycondensation was confirmed by the presence of methylene ether and methylene groups – e.g. CH₂–O–CH₂ at ca. 68 and 53 ppm and CH₂ at ca. 31 and 24 ppm – linking adjacent aromatic rings through 4-4' and 2-4' positions.^{78, 79} The signal at ca. 120-121 ppm was also interesting in terms of condensation since it corresponds to aromatic carbons of mono- and disubstituted R molecules bearing CH₂ groups in all ortho positions relative to the phenolic OHs. Non-substituted aromatic CH groups in meta positions appeared at 131 ppm. Both the signals ascribed to methylene and methylene ether groups, and the signals at ca. 120-121

and 131 ppm exhibited similar intensities for all the samples, thus revealing basically identical polycondensation degrees in every case.

Resins were thermally treated at 800 °C in N₂ atmosphere for the formation of the respective carbons with good conversions – i.e. in range to those reported for previous DES-assisted condensations⁶¹⁻⁶⁵ – (Table 3) as anticipated by FTIR and ¹³C CPMAS NMR spectroscopies. The carbonization of unwashed resins produced carbons with significant nitrogen and phosphorus contents (Table 3). The textural properties of C_{RPGC80}, C_{RPGC40} and C_{RPGC20} were studied by gas adsorption – N₂ at –196 °C and CO₂ at 0 and 25 °C – and Hg porosimetry (Figure 3 and Figure S4, respectively). N₂ adsorption–desorption isotherms were type I with a sharp increase in adsorption at low relative pressures that is characteristic of microporous materials (Figure 3a). Table 4 summarizes the Brunauer–Emmett–Teller surface area, the micropore volume and the pore size distributions (PSDs) of micro- and macropores – i.e. obtained from the analysis of the isotherms using the Barrett–Joyner–Halenda (BJH) method in the former case, and from Hg porosimetry in the latter one. CO₂ adsorption–desorption isotherms also confirmed the presence of a narrow microporous network throughout every RPGC carbon (Figure 3b). Moreover, the CO₂ adsorption capacity was remarkable at both 0 and 25 °C, with uptakes at 760 mbar that were in range to or even better than some of the most remarkable sorption capacities found for microporous carbons of different natures – see in Table 5 examples of non-doped, doped, and co-doped carbons in either non-activated or activated form.^{80, 81, 82, 83, 84, 85, 86}

At this stage, we investigated the morphology of the different carbons by SEM. SEM micrographs revealed how the morphologies changed remarkably with the increase of the mass fraction of water during polycondensation. Thus, C_{RPGC80} exhibited a fine bicontinuous structure (Figure 4). Meanwhile, C_{RPGC70} exhibited a bicontinuous structure as well, but with a thicker skeleton as compared to R_{RPGC80} (Figure 4). The SEM micrographs of C_{RPGC70} also revealed the presence of both small spherical pores – of about 0.5-1 µm – in the coarse skeleton and small particles – of about 0.5-1 µm – within the open porosity that ultimately landed on the surface of the skeleton after the removal of the non-condensed matter – i.e. by drying and subsequent carbonization. The spherical pores were voids left by the solvents that, during polycondensation, separated out in the polymer-rich domain as a result of the secondary phase separation. Secondary phase separation is the precipitation of a phase within a phase, and can occur when a region of a phase-separated microstructure is physically isolated and develops further immiscibility.^{29, 30, 50, 51} Secondary phase separation may occur in the polymer phase, in the pore phase or in both, as it actually occurred in our case. Further increase of the mass fraction of water during polycondensation provided morphologies to C_{RPGC60}, C_{RPGC50}, C_{RPGC40}, C_{RPGC30}, and C_{RPGC20} characterized by loosely packed isolated spheres, the mean size of which became larger along with the increase of water content because of the occurrence of further particles growth for long gelation times (Figures 4 and Figure S5).

Study of starting DES/H₂O binary mixtures

As described above, the aim of this work was also studying the starting DES/H₂O binary solutions so that one could predict the suitability of these solutions in SD processes. The above-described results with regard to SD processes during the polycondensation of DES/H₂O binary mixtures reconciled with previously described chemically induced phase separations where immiscibility is observed to develop concurrently with polymerization, and the ultimate morphology of the resulting polymer depends on the onset between phase separation and gel formation. In every SD process reported to date, the fluid phase resulting after phase separation is a solvent mixture that contains the PSIA, the co-solvent that helps to demix the PSIA – note co-solvents might be used or not – and any additional compound that may result as a by-product of the reaction.¹⁴ In our particular case, the fluid phase was composed of the non-polymerizable DES components – e.g. P, G and C – and H₂O. The former were originally part of the DES, the rupture of which during polycondensation resulted in their segregation to the fluid phase. With regard to H₂O, a minor fraction of it was the by-product of RF polycondensation but most of it was added at the starting homogeneous solution and promoted/favoured phase separation. The use of water as PSIA has been rarely described in papers dealing with SD processes^{41, 42, 43, 50} despite the obvious interest that its use offers in environmental and sustainable terms as compared to other co-solvents more commonly used – e.g. non-friendly solvents, polymers and/or surfactants. As described previously,⁵⁰ the mass fraction of water controls the resulting morphology in terms of reaction kinetics. Thus, in diluted samples, phase separation occurs earlier than gel formation so that the polymer-rich domains break-up into spherical colloids that, afterwards, become a gel – i.e. sooner for pseudo-diluted samples and later for highly diluted ones (Figure S6).

It is also worth noting a peculiarity of these DES-assisted SD processes with regard to the role of water as PSIA. As in any regular SD processes, the macroscopic appearance of our starting solutions – aqueous dilutions of DES – was homogeneous (Figure 1). In our case, all the DES components are soluble in water so, in these cases, it is commonly assumed that the resulting DESs are entirely water miscible as well.⁸⁷ However, recent reports describe how the scenery that results from aqueous dilution of DES is not yet fully understood by the research community.⁸⁸ For instance, DESs prepared from water-soluble components will tend to become a simple solution of the individual components at high dilutions⁸⁹ so there are at least two questions that arise; (1) what is the dilution threshold at which DES fully breaks into its respective counterparts? and (2) what sort of solution do we have for intermediate water contents?

With regard to the first question, we have demonstrated in some of our previous works that ¹H NMR spectroscopy is a useful tool to get insights about DES rupture upon dilution.⁷³⁻⁷⁶ As mentioned above, DESs result from the formation of the halide ion-hydrogen-bond-donor supramolecular complexes between two or more molecules, being at least one of them a HBD and another one a HBA. The formation of H-bond complexes typically occurs through the most labile protons that exist in the component acting as HBD. For

instance, H-bond complex in one of the most studied DES – e.g. DES_{UC}, composed of urea (U) and C, and combined in a 2:1 molar ratio – are suggested to occur via interactions between the NH₂ groups of U and the chloride ion of C.^{90, 91, 92} More recently, different studies based on neutron diffraction experiments and atomistic modelling have confirmed that each chloride is H-bonded to two U molecules.^{93, 94} Interestingly, these works also described how, once chloride ion is stabilized by U and to better accommodate U within the H-bond complex, most chloride ions are positioned near the OH group of the choline cation. Thus, the H-bond complex involves one choline, one chloride and two urea molecules, being the H-bonding between the NH₂ groups of U and the chloride ion stronger than that between the OH group of the choline cation and the chloride ion.

The above-described different role that each particular labile proton plays in the H-bond complex is actually in agreement with some ¹H NMR spectroscopic results we published in a previous work.⁷⁵ In neat DES_{UC}, we could see how labile protons at the OH group of C and at the NH₂ groups of U were not exchangeable among themselves and produced their respective signals in the spectrum – i.e. at 4.7 and 5.6 ppm. Interestingly, subsequent experiments in D₂O-diluted DESs revealed that labile protons at the OH group of the choline cation were fully exchanged with D₂O for DESs contents above 86 wt% whereas labile protons at the NH₂ groups of U needed of further dilution to become fully exchangeable – i.e. for DESs contents below 43 wt% (Figure 5a). In view of these results, we also hypothesized that DES_{UC} fully breaks into its respective counterparts – so it become a solution of the individual components – when all the labile protons are fully exchanged with D₂O as it happens in any regular solution.

The ¹H NMR spectra of DES_{RPGC} in both its neat and diluted form was also illustrative with regard to the dilution range at which DES is fully broken into its respective components. Nonetheless, DES_{RPGC} revealed a different behaviour than that described above for DES_{UC}. In neat form, all the labile protons – e.g. coming from OH groups of resorcinol and glycerol, as well as from H₃PO₄ – exchanged among themselves – as revealed their appearance as a single signal at 7.5 ppm – indicating an equal H-bonding participation for every one in the H-bond complex (Figure S2 and Table S2 at Supporting Information). Upon dilution with D₂O, the signal assigned to labile protons of DES components evolved – in an up-field-shifting fashion – aiming to meet the signal of HDO located at ca. 4.7 ppm (Figure 5b). In structural terms, it is plausible correlating this shifting with the size of H-bond domains.^{95, 96} In our case, the occurrence of proton exchange must indeed be favoured as DES domains become smaller because of the increase of the surface interface with the surrounding D₂O. Interestingly, two separate signals yet remained for highly diluted samples – ca. 10 wt% – so we could assume that DES_{RPGC} was not fully broken and some tiny DES-domains yet remain even at that dilution.

With regard to the second question, it is worth reminding the idea of cooperativity of H-bonding in water to ultimately form 3-D H-bonded networks. Briefly, the formation of a first H-bond results in a change

in the charge distribution within the first participating unit in such a way that the hydrogen acceptor molecule becomes potentially an even better H-bond donor than before and it is thus capable of forming a stronger second bond because of the existence of the first one. The same is true for the proton donor, which has an enhanced ability to accept a proton as a result of the bond that it has already formed.⁹⁷ More interestingly, it is widely accepted the occurrence of amorphous polymorphism – polyamorphism – at ambient conditions, this is liquid water (with average density 1 g/cm³) fluctuating permanently between low-density liquid (LDL, density 0.94 g/cm³) and high-density liquid (HDL, density 1.14 g/cm³) clusters.⁹⁸ Phase separation between them and liquid-liquid polyamorphous transition have been predicted by numerical modelling⁹⁹ but its experimental observation has only been possible in aqueous solutions of salts^{100, 101} or H-bond-forming molecules – e.g. polyols, sugars, etc.^{102, 103} It is worth noting that liquid-liquid transitions without macroscopic phase separation has also been observed in water-glycerol mixtures.¹⁰⁴

Protic ILs are reminiscent of water and hence capable to form 3-D H-bonded networks in both neat form and aqueous dilutions.¹⁰⁵ Actually, aqueous solutions of hydrophilic ILs can also result in the formation of aqueous biphasic systems upon the addition of a kosmotropic – water structuring – salt.^{106, 107} Moreover, the formation of mesoscopic nanostructures – as either isolated globular islands within the continuous polar network or sponge-like bicontinuous structures – has been reported by number of authors and recently summarized by Atkin and coworkers in an excellent review.¹⁰⁸

DEs also belong to the group of H-bond-forming molecules and recent works dealing with pseudo-concentrated aqueous solutions of DES_{UC} have demonstrated the interstitial accommodation of water within the DES-based 3D H-bonded network.¹⁰⁹ Actually, ternary and quaternary eutectic mixtures could eventually be formed upon the incorporation of stoichiometric water to the original DES.⁸⁸ Uncertainty yet remains at intermediate dilutions where the water fraction is too high for being fully accommodated within the DES and too low for fully promote the DES rupture and dissolve its components. In these intermediate cases, one could hypothesize about the presence of two 3D H-bonded networks – i.e. a DES-based 3D H-bonded network eventually containing some water molecules and an aqueous-based one eventually containing a minor fraction of the original DES components coming from partial DES rupture – phase separated at the nanoscale of the macroscopically homogeneous DES/H₂O binary mixture.¹¹⁰

Elucidating whether this was the situation in the aqueous solutions of RPGC described in this work was performed by Brillouin light-scattering experiments. This experimental technique focuses on the analysis of the light inelastically scattered on the thermally induced sound waves (phonons), that propagate through a medium at a velocity that depends on the sample density and rigidity (expressed in terms of the storage longitudinal modulus). Brillouin spectroscopy has been used to determine acoustic velocities and elastic properties of a number of crystalline solids, glasses, and liquids. Within the context of this work, particularly interesting is the use of Brillouin spectroscopy for studying liquid mixtures of H-bond co-solvents – e.g.

methanol (MeOH), ethanol (EtOH), propanol (PrOH), or tert-butanol (t-BuOH), among others – and even polymers – e.g. polyethyleneglycol (PEG) – with either water or organic solvents.^{111, 112, 113, 114, 115, 116, 117, 118, 119}

The spectrum associated with a binary solution consists of three peaks; the central one resulting from Rayleigh scattering and lacking of interest in this case, and the two Brillouin peaks located at frequencies $\omega = \pm k v_H(f)$ – referred to the Rayleigh one, where k denotes the absolute value of the wave vector transfer, f is the frequency of the sound wave and v_H the hypersonic velocity. Interestingly, a deviation from the ideal behaviour has been observed in binary liquid mixtures when representing the v_H obtained from Brillouin scattering measurements versus the molar fraction (χ) of one of the components, thus revealing that these binary mixtures are inhomogeneous on a microscopic molecular level regardless their fully miscible appearance in macroscopic terms.

Local structure rearrangements resulting from non-ideal mixing in binary mixtures have been also observed by molecular simulations and, experimentally, by ^1H NMR spectroscopy. For instance, in EtOH/ H_2O mixtures, molecular simulations have revealed the occurrence of a certain structural transition from EtOH's clustering to micro-segregated distributions of H_2O and EtOH domains forming a co-continuous structure within a particular range of χ_{EtOH} – e.g. $0.15 < \chi_{\text{EtOH}} < 0.5$. Interestingly, the χ_{EtOH} where structural rearrangements occur coincided with that where the labile protons of H_2O and EtOH were not longer exchanged in the ^1H NMR spectra^{112, 120, 121} and with that where the v_H obtained from Brillouin spectroscopy reached a sharp maximum.¹¹¹ It is worth noting that this trend in v_H is common for MeOH/ H_2O , t-BuOH/ H_2O and PEG/ H_2O binary mixtures with just slight variations with regard to the plot shape and the χ at which the maximum is reached. Thus, in PEG/ H_2O binary mixtures, the v_H maximum was reached at $\chi_{\text{PEG}} \approx 0.5$ and decreased just smoothly within the $0.5 < \chi_{\text{PEG}} < 1$ range because of the slight difference between this one and that reached in neat PEG (Figure 7a).¹¹⁴ Quite different is the v_H -vs- χ plot of binary mixtures where the solvent is not a H-bond liquid and it is rather a weakly interacting one. For instance, the v_H -vs- χ plot of MeOH/ CCl_4 binary mixtures displayed a minimum rather than the maximum displayed in MeOH/ H_2O binary mixtures (Figure 7a).¹¹⁷ This behaviour is ascribed to the different rigidity change experienced by the binary mixtures at low co-solvent concentrations depending on their aqueous or organic character; i.e. increasing in the former case because of the strong H-bond interactions between the solvent and the co-solvent, and decreasing in the latter one because of the weak interactions between the solvent and the co-solvent. Moreover, the shape of the v_H -vs- χ plot can evolve in some particular organic binary mixtures – e.g. PEG/ CCl_4 ¹¹⁸ or PEG/toluene¹¹⁹ – so that, rather than a minimum, the plot displays a monotonic increase of v_H along with χ_{PEG} , the slope of which becomes steeper for certain χ_{PEG} values where percolation of originally isolated polymer clusters results in the formation of a continuous polymer network throughout the entire 3D mixture (Figure 7a).

In our case, the shape of the ν_H -vs- χ plot of DES/H₂O binary mixtures resembled that displayed by PEG/H₂O binary mixtures (Figure 7b). Assuming our DES/H₂O binary mixtures behaves as those previously discussed, the χ_{DES} at which the slope changes reports on the formation of a co-continuous structure, evolving from a situation for low χ_{DES} values where isolated DES domains are dispersed within a continuous H-bond network of H₂O. The presence of DES domains even at very low χ_{DES} values was actually confirmed by ¹H NMR spectroscopy (see above, Figure 6b). Interestingly, representing ν_H versus DES content in wt%, the plot was even clearer in this regard, now exhibiting two well-distinguishable regions when transitioning from the ν_H of neat H₂O to that of neat DES – e.g. xx and yy m/s, respectively. Thus, in the region of low DES contents, sound waves travelled at ν_H near to or just slightly above that of H₂O, as consequence of the presence of yet-isolated DES domains that force sound to propagated through the continuous H-bond network of H₂O. Meanwhile, above a certain threshold value of DES content, the plot of ν_H -vs-DES content in wt% now exhibited a second region where ν_H approached that of neat DES in a quicker fashion, indicating the coalescence of DES domains into a continuous network structure through which sound now propagates more favourably. Based on this, nanostructural features of DES/H₂O binary mixtures along the whole range of DES contents could be represented, in an idealized fashion, as in Figure 8. Esto ultimo no se si va o no...

Conclusions

We have demonstrated the capability of aqueous solutions of DESs for the preparation of porous carbons via SD – and subsequent carbonization – so that the resulting structure just depends on the DES dilution. In particular, SEM micrographs allowed distinguishing the transition from bicontinuous morphologies – this is those in which both phases are smoothly interconnected in three dimensions – to bicontinuous with secondary phase separation – with both isolated pores in the polymer phase and particles in the pore phase – up to aggregates-of-particle morphologies – which can nonetheless be interconnected due to packing considerations – when the mass fraction of water increased. The microporosity of some of these carbons was particularly effective for CO₂ capture with absorptions of up to 4.7 mmol/g at 0 °C and 760 mbar. More interestingly, we have also investigated whether Brillouin spectroscopy can be used to predict the suitability of a particular aqueous solution of DES to undergo the SD process. Brillouin spectroscopy was chosen given its capability to observe local structure rearrangements resulting from non-ideal mixing. In practical terms, we observed that the range of DES contents for which an aqueous solution of DES demix into a co-continuous structure coincided with a discontinuity of the linearity in the plot of ν_H versus DES content. According to these results, Brillouin spectroscopy was capable of predicting not only the suitability of a particular solution for the preparation of carbons via SD processes but also the range of dilutions for which every morphology – e.g. bicontinuous- or aggregates-of-particle-like – will be ultimately obtained.

Acknowledgements

This work was supported by MINECO (Project Numbers MAT2012-34811, MAT2012-37276-C03-01 and MAT2015-68639-R).

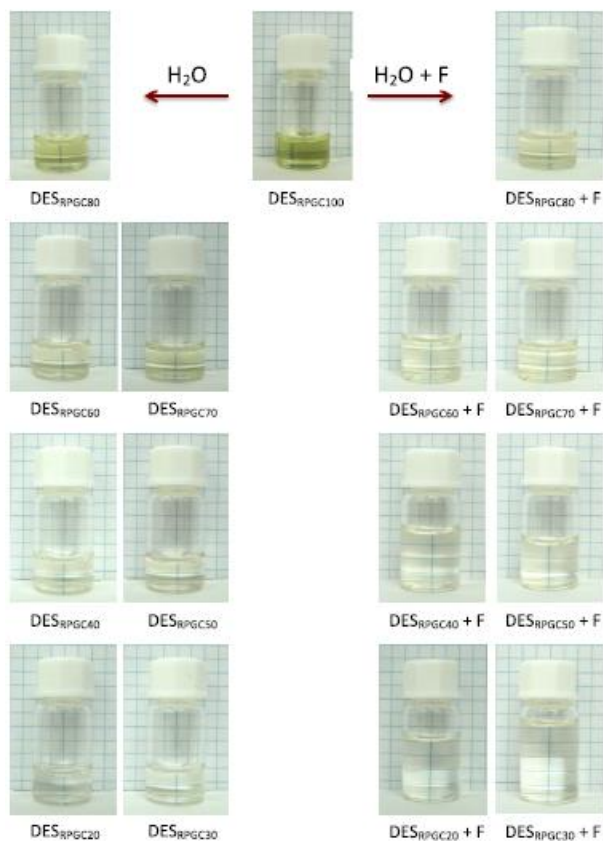


Figure 1 – Picture of $\text{DES}_{\text{RPGC100}}$ and the different aqueous solutions used in this work – diluted with just H_2O (left) or with H_2O and F added for polycondensation (right).

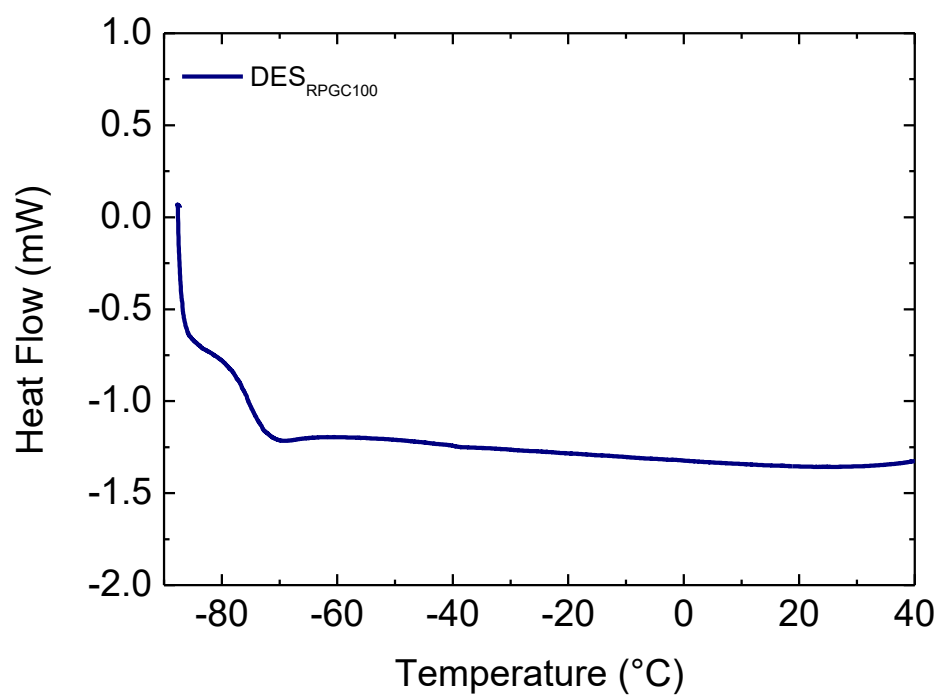


Figure 2 – DSC scan of DES_{RPGC}. The scan rate was 5°C/min.

Figure 3 – SEM micrographs of some representative C_{RPGC} samples obtained after polycondensation.

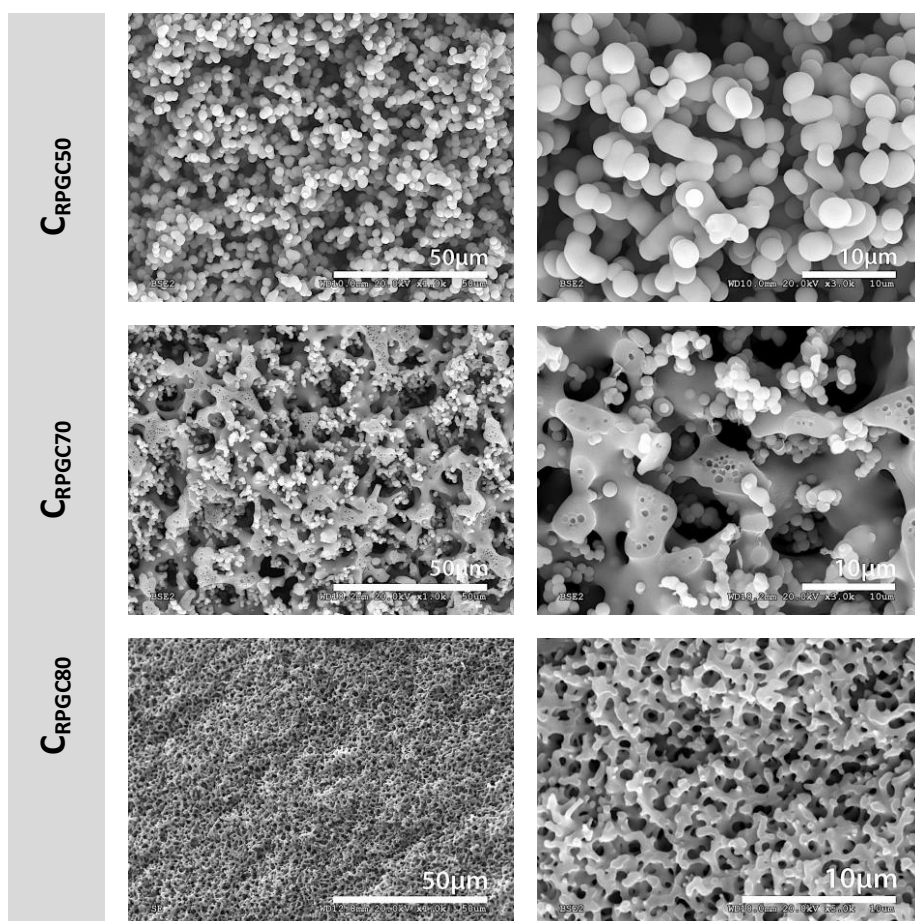


Figure 4 – (a) Plot of hypersonic velocity versus molar fraction of co-solvent for different binary mixtures. Adapted from references 111, 112, 114, 117, and 118. (b) Plot of hypersonic velocity versus the molar fraction of DES (solid purple squares) and versus the mass content of DES (solid orange triangles) in the DES/H₂O binary mixtures studied in this work.

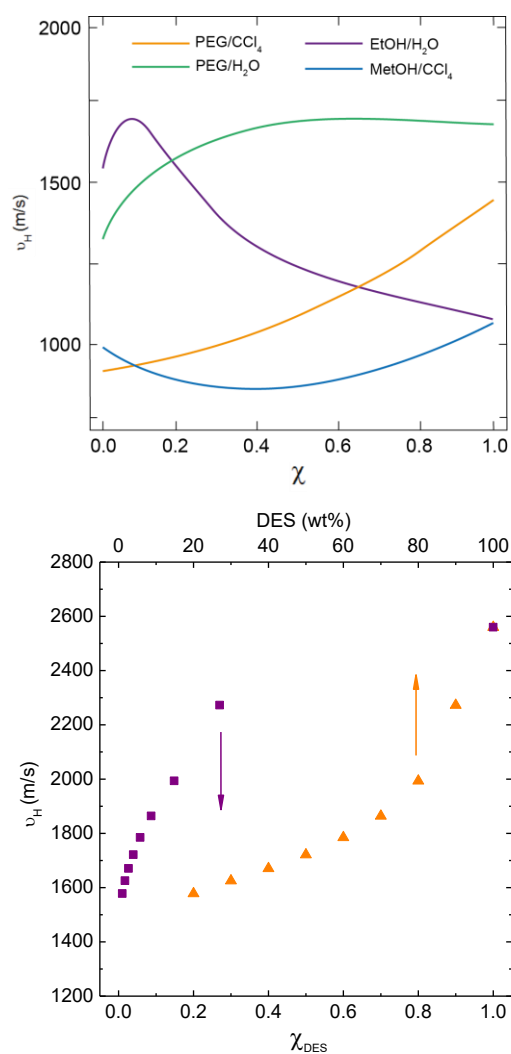


Figure 5 – Plot representing the evolution of the chemical shifts of labile exchangeable protons upon aqueous dilution of DES_{RPGC100} k.

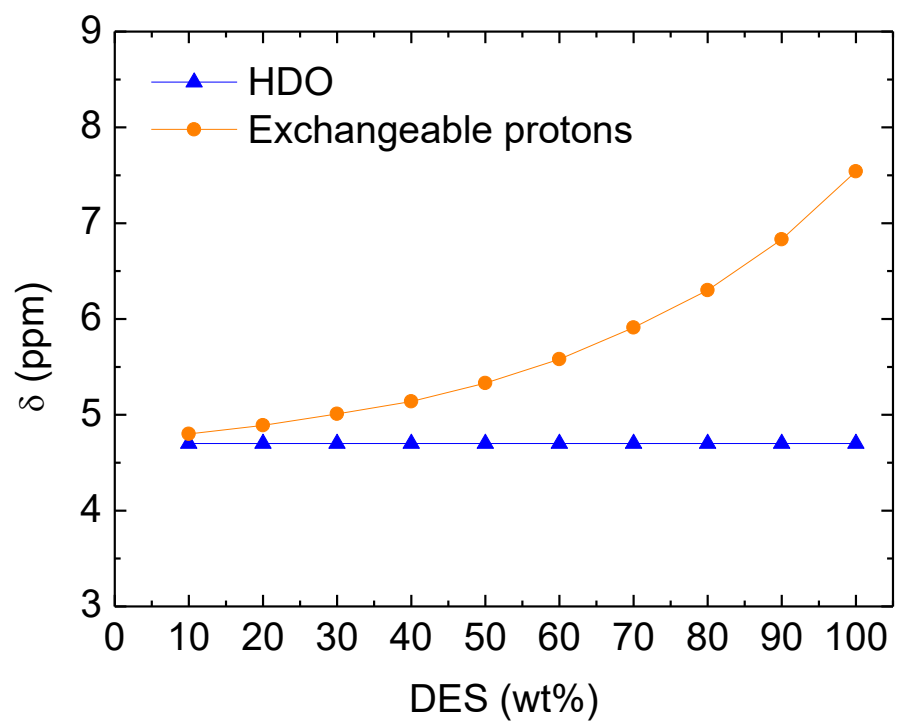


Figure 6 -6. Idealized scheme representing the formation of aggregates-of-particles or spinodal morphologies in regular and DES-assisted phase separation processes. In the particular case of DES-assisted phase separation processes, transition from aggregates-of-particles to spinodal morphologies is obtained upon the use of DES/H₂O binary mixtures with increased DES contents. As compared to regular SD processes, Brillouin spectroscopy has revealed that the macroscopically homogenous starting solution exhibit certain heterogeneities at the nanoscale e i.e. DES nanodomains, first isolated for low DES contents and then forming a bicontinuous structure for increased DES contents. Considering that DES nanodomains are rich in resorcinol, first nucleation and growth of colloidal particles will occur preferentially at these positions so that phase separation is anticipated as compared to regular SD processes.

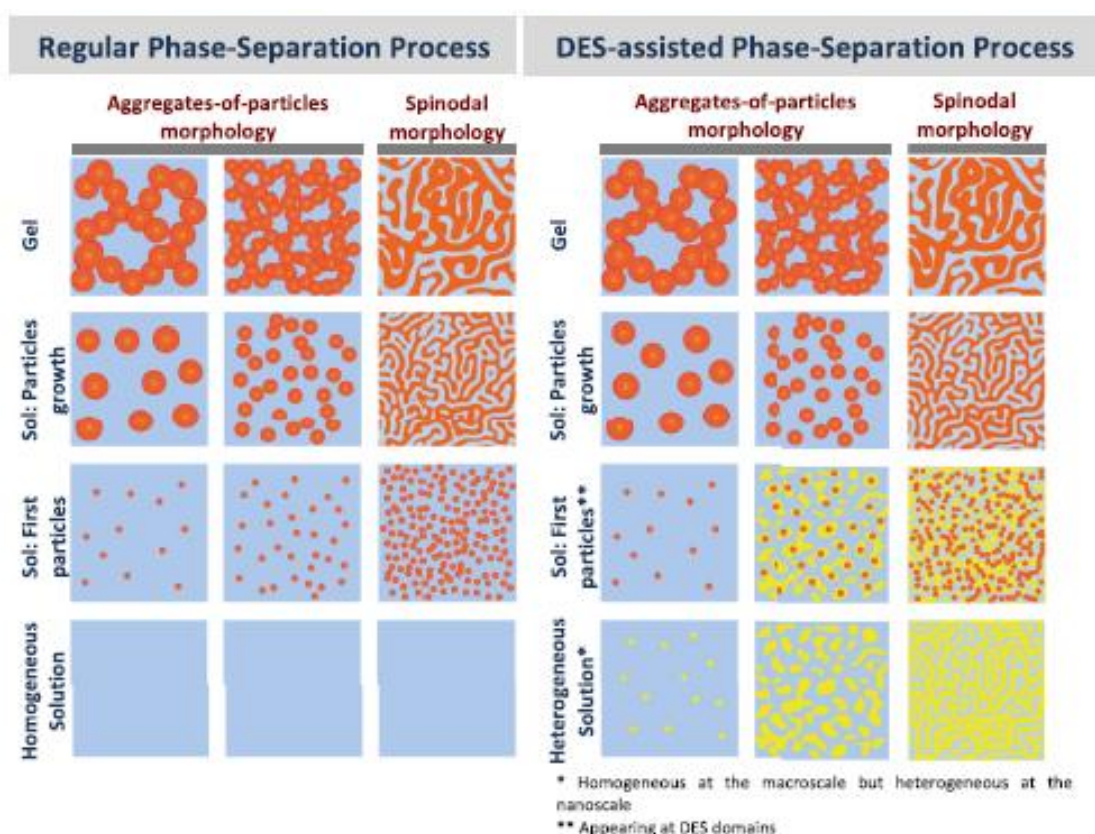


Figure 7 – N₂ (a) and CO₂ (b) adsorption/desorption isotherms of C_{RPGC80}, C_{RPGC60} and C_{RPGC20} at, respectively, – 196 °C (solid symbols), and at 0 (solid symbols) and 25 °C (only for C_{RPGC60} and C_{RPGC20}, open symbols).

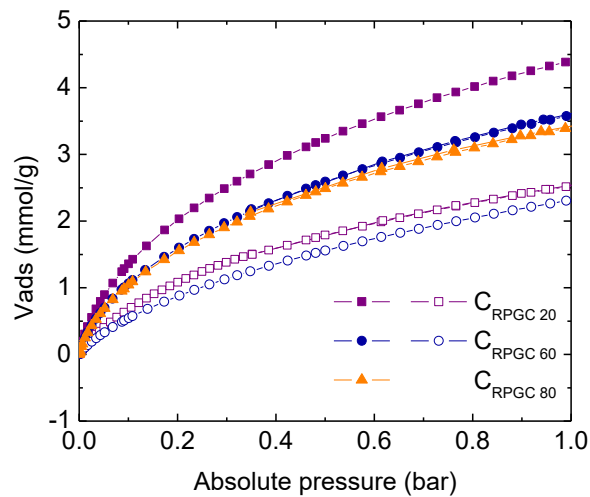
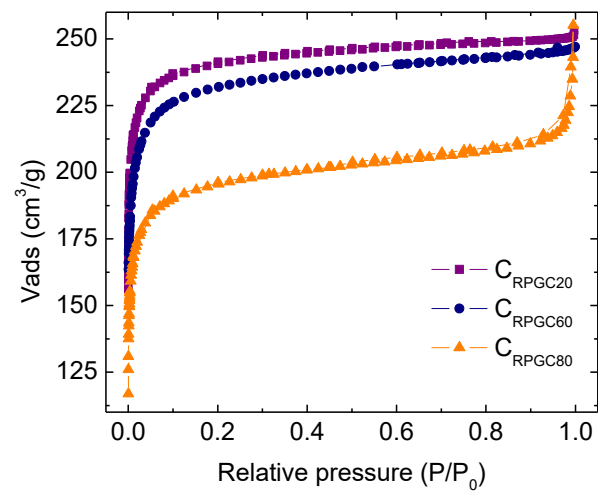


Table 1: Reagents – and their corresponding amounts in mg – used for the preparation of DES_{RPGC} and its respective dilutions, as well as for the polycondensation of these samples with formaldehyde.

Sampl e	R	P	G	C	DES _{RPGC}	F	H ₂ O ^a	H ₂ O ^c
DES _{RPG} C100	6 75	6 02	5 65	8 59	2701 (100 wt%)	--	--	--
DES _{RPG} C80	6 75	6 02	5 65	8 59	2701 (80 wt%) ^b	3 73	635 ^d (20 wt%) ^b	--
DES _{RPG} C70	6 75	6 02	5 65	8 59	2701 (70 wt%) ^b	3 73	1158 (30 wt%) ^b	50 5
DES _{RPG} C60	6 75	6 02	5 65	8 59	2701 (60 wt%) ^b	3 73	1807 (40 wt%) ^b	11 72
DES _{RPG} C50	6 75	6 02	5 65	8 59	2701 (50 wt%) ^b	3 73	2715 (50 wt%) ^b	20 80
DES _{RPG} C40	6 75	6 02	5 65	8 59	2701 (40 wt%) ^b	3 73	4051 (60 wt%) ^b	34 16
DES _{RPG} C30	6 75	6 02	5 65	8 59	2701 (30 wt%) ^b	3 73	6300 (70 wt%) ^b	56 65
DES _{RPG} C20	6 75	6 02	5 65	8 59	2701 (20 wt%) ^b	3 73	10805 (80 wt%) ^b	10 170

^a Total amount of H₂O in the DES/H₂O binary mixture. ^b The weight percent of DES and H₂O – considering the sum of the mass of DES and H₂O as 100% – is included between brackets. ^c Additional H₂O added to that coming from the F aqueous solution to obtain the desired wt%.

Table 2: Conversions in which resins became carbons after carbonization at 800 °C in nitrogen atmosphere. The nitrogen and phosphorus contents found in the resulting carbons by TXRF, elemental analysis and XPS –in this case for CRPGC80, CRPGC60 and CRPGC20 are also included.

Sample	Conversion (wt%)	Nitrogen	Phosphorus	Pyridi	Pyrrol	Q
		Content (wt% ^a)	Content (wt% ^a)	nic-N	ic-N	uaternary-
		at	at	Content	Content	N Content
		(%) ^c	(%) ^c	(%) ^d	(%) ^d	(%) ^d
C _{RPG} C80	50	2.68 ^a	5.52 ^b	17.5	38.7	33.8
C _{RPG} C70	56	2.63 ^a	6.10 ^b	-	-	-
C _{RPG} C60	63	2.63 ^a	5.40 ^b	25.7	41.8	26.4
C _{RPG} C50	58	2.58 ^a	5.23 ^b	-	-	-
C _{RPG} C40	61	2.83 ^a	6.87 ^b	-	-	-
C _{RPG} C30	52	2.62 ^a	5.22 ^b	-	-	-
C _{RPG} C20	60	2.59 ^a	5.65 ^b	30.4	42.1	21.9

^a As obtained from TXRF.

^b As obtained from elemental chemical analysis.

^c As obtained from XPS.

^d Referred to the

overall N content found by XPS.

Table 3: Summary of data obtained from N₂ adsorption/desorption isotherms at – 196 °C and Hg porosimetry for C_{RPGC80}, C_{RPGC60} and C_{RPGC20} carbons.

Sample	S_{BET} (m^2/g) ^a	Total	Micropore	Pore Diameter (nm)	
		Volume (cm^3/g) ^b	Volume (cm^3/g) ^c		
C _{RPG} C80	780	0.36	0.302	0.63 _d	1050 ^e
C _{RPG} C60	930	0.38	0.367	0.64 _d	3520 ^e
C _{RPG} C20	976	0.39	0.370	0.65 _d	19000 ^e

^a Applying the BET equation to the N₂ adsorption isotherms. ^b Determined at $p/p \approx 0.99$.

^c Determined using the Dubinin–Radushkevich equation applied to the N₂ adsorption data.

^d Averaged narrow micropore size determined applying the Stoeckli–Ballerini equation to the CO₂ adsorption data. ^e Averaged macropore size determined from Hg porosimetry.

Table 4: CO₂ uptake at 0 and 25 ° found for C_{RPGC80}, C_{RPGC60} and C_{RPGC20} carbons, and for some of the most remarkable microporous carbons – bare, nitrogen-doped and phosphorus-doped – recently reported. The nitrogen and phosphorus contents of doped- and co-doped carbons provided in the different works are also included.

Sample	Reference	Nitrogen/Phosphorus content (wt%)	CO ₂ -uptake at 25/0 °C (mmol/g)
C _{RPGC80}	This work	2.7/5.5	--/3.7
C _{RPGC60}	This work	2.8/5.4	2.5/3.9
C _{RPGC20}	This work	2.6/5.7	2.8/4.7
C _{ReHy12@800}	76	3.7/--	2.7/3.7
C _{ReHy13@800}	76	5.4/--	2.7/3.6
N _{3C@800}	77	3.8/--	3.3/4.2
C200-180	80	--/--	2.2/3.0
IBN9-NC1	81	16.1/--	1.8/2.5
IBN9-NC1A ^a	81	12.9/--	4.5/6.5

KNC-A-K ^a	82	17.4/--	4.0/5.1
SBA-NC	82	10.5/--	2.3/3.0
SBA-C-A-K ^a	82	10.5/--	2.3/3.3
AC2-635 ^b	83	4.6/--	3.9/6.0
CP2-600 ^c	84	10.1/--	3.9/6.2
CP2-800	84	0.8/--	2.7/4.3
PAC800	85	6.1/--	2.3/3.0
PAC50/800	85	5.6/0.5 ^d	2.5/4.2
PAC150/800	85	6.3/0.7 ^d	2.5/5.0
PAC900	85	5.5/--	2.3/3.3
PAC50/900	85	7.0/4.6 ^d	1.8/4.0
PAC150/900	85	8.9/5.4 ^d	1.8/3.6
P1	86	--/P-doped ^e	2.5/--

^a Submitted to KOH activation. ^b Carbonized at 635 °C. ^c Carbonized at 600 °C. ^d Obtained from XPS. ^e Data with regard to the wt% is not given in the publication

References

- ¹ R. E. Morris, P. S. Wheatley, "Gas storage in nanoporous materials" *Angew. Chem.* **2008**, *47*, 4966–4981.
- ² C. Moreno-Castilla, F. J. Maldonado-Hódar, "Carbon aerogels for catalysis applications: An overview" *Carbon* **2005**, *43*, 455–465.
- ³ Z.-W. Liu, F. Peng, H.-J. Wang, H. Yu, W.-X. Zheng, J. Yang, "Phosphorus-doped graphite layers with high electrocatalytic activity for the O₂ reduction in an alkaline medium" *Angew. Chem.* **2011**, *50*, 3257–3261.
- ⁴ E. Frackowiak, "Carbon materials for supercapacitor application" *Phys. Chem. Chem. Phys.* **2007**, *9*, 1774–1785.
- ⁵ Y.-S. Hu, P. Adelhelm, B. M. Smarsly, S. Hore, M. Antonietti, J. Maier, "Synthesis of Hierarchically Porous Carbon Monoliths with Highly Ordered Microstructure and Their Application in Rechargeable Lithium Batteries with High-Rate Capability" *Adv. Funct. Mater.* **2007**, *17*, 1873–1878.
- ⁶ S. Simovic, D. Losica, K. Vasilev, "Controlled drug release from porous materials by plasma polymer deposition" *Chem. Commun.* **2010**, *46*, 1317–1319
- ⁷ B. Hu, K. Wang, L. Wu, S.-H. Yu, M. Antonietti, M.-M. Titirici, "" *Adv. Mater.* **2010**, *22*, 813–828
- ⁸ M. Sevilla, A. B. Fuertes, "" *Chem. Eur. J.* **2009**, *15*, 4195–4203.
- ⁹ Y. Huang, H. Cai, D. Feng, D. Gu, Y. Deng, B. Tu, H. Wang, P. A. Webley, D. Zhao, "" *Chem. Commun.* **2008**, 2641–2643
- ¹⁰ C. Liang, K. Hong, G. A. Guiochon, J. W. Mays, S. Dai, "" *Angew. Chem.* **2004**, *116*, 5909
- ¹¹ L. Chuenchom, R. Kraehnert, and B. M. Smarsly "Recent progress in soft-templating of porous carbon materials" *Soft Matter* **2012**, *8*, 10801
- ¹² G. Hasegawa, K. Kanamori, K. Nakanishi, and T. Hanada, "Hierarchically porous carbon monoliths with high surface area from bridged polysilsesquioxanes without thermal activation process" *Chem. Commun.* **2010**, *46*, 8037.
- ¹³ G. Hasegawa, K. Kanamori, K. Nakanishi, and T. Abe, "New Insights into the Relationship between Micropore Properties, Ionic Sizes, and Electric Double-Layer Capacitance in Monolithic Carbon Electrodes" *J. Phys. Chem. C* **2012**, *116*, 26197.
- ¹⁴ K. Nakanishi and N. Tanaka, "Sol–Gel with Phase Separation. Hierarchically Porous Materials Optimized for High-Performance Liquid Chromatography Separations" *Acc. Chem. Res.* **2007**, *40*, 863.
- ¹⁵ C. Triantafillidis, M. S. Elsaesser and N. Hüsing, "Chemical phase separation strategies towards silica monoliths with hierarchical porosity" *Chem. Soc. Rev.* **2013**, *42*, 3833.
- ¹⁶ L. Li, X. Shen, S. W. Hong, R. C. Hayward, and T. P. Russell, "Fabrication of Co-continuous Nanostructured and Porous Polymer Membranes: Spinodal Decomposition of Homopolymer and Random Copolymer Blends" *Angew. Chem. Int. Ed.* **2012**, *51*, 4089.
- ¹⁷ H. Kaji, K. Nakanishi, N. Soga, T. Inoue, and N. Nemoto, "In Situ Observation of Phase Separation Processes in Gelling Alkoxy-Derived Silica System by Light Scattering Method" *J. Sol-Gel Sci. Technol.* **1994**, *3*, 169.
- ¹⁸ H. Kaji, K. Nakanishi, N. Soga, T. Inoue, and N. Nemoto, "Phase Separation in Silica Sol-Gel System Containing Poly(ethylene oxide) II. Effects of Molecular Weight and Temperature" *Bull. Chem. Soc. Jpn.* **1997**, *70*, 587.

-
- ¹⁹ Y. Gao, J. Kim and M. E. Helgeson, "Microdynamics and arrest of coarsening during spinodal decomposition in thermoreversible colloidal gels" *Soft Matter*. **2015**, *11*, 6360.
- ²⁰ K. Nakanishi, Y. Kobayashi, T. Amatani, K. Hirao, T. Kodaira, "Spontaneous Formation of Hierarchical Macro-Mesoporous Ethane-Silica Monolith" *Chem. Mater.* **2004**, *16*, 3652–2658
- ²¹ T. Amatani, K. Nakanishi, K. Hirao, T. Kodaira, "Monolithic Periodic Mesoporous Silica with Well-Defined Macropores" *Chem. Mater.* **2005**, *17*, 2114–2119
- ²² K. Nakanishi, T. Amatani, S. Yano, and T. Kodaira, "Multiscale Templating of Siloxane Gels via Polymerization-Induced Phase Separation" *Chem. Mater.* **2008**, *20*, 1108
- ²³ K. Kanamori, K. Nakanishi, and T. Hanada, "Spinodal decomposition in siloxane sol-gel systems in macroporous media" *Soft Matter*. **2009**, *5*, 3106.
- ²⁴ J. Konishi, K. Fujita, S. Oiwa, K. Nakanishi, and K. Hirao, "Crystalline ZrO₂ Monoliths with Well-Defined Macropores and Mesoporous Skeletons Prepared by Combining the Alkoxy-Derived Sol–Gel Process Accompanied by Phase Separation and the Solvothermal Process" *Chem. Mater.* **2008**, *20*, 2165
- ²⁵ M. Kurahashi, K. Kanamori, K. Takeda, H. Kajib, and K. Nakanishi, "Role of block copolymer surfactant on the pore formation in methylsilsesquioxane aerogel systems" *RSC Adv.* **2012**, *2*, 7166.
- ²⁶ A. Kitada, G. Hasegawa, Y. Kobayashi, K. Kanamori, K. Nakanishi, and H. Kageyama, "Selective Preparation of Macroporous Monoliths of Conductive Titanium Oxides Ti_nO_{2n-1} (n = 2, 3, 4, 6)" *J. Am. Chem. Soc.* **2012**, *134*, 10894.
- ²⁷ Y. Kido, K. Nakanishi, and K. Kanamori, "Sol–gel synthesis of zinc ferrite-based xerogel monoliths with well-defined macropores" *RSC Adv.* **2013**, *3*, 3661.
- ²⁸ N. Moitra, K. Kanamori, T. Shimada, K. Takeda, Y. H. Ikuhara, X. Gao, and K. Nakanishi, "Synthesis of Hierarchically Porous Hydrogen Silsesquioxane Monoliths and Embedding of Metal Nanoparticles by On-Site Reduction" *Adv. Funct. Mater.* **2013**, *23*, 2714.
- ²⁹ X. Guo, W. Li, K. Nakanishi, K. Kanamori, Y. Zhu, and H. Yang, "Preparation of mullite monoliths with well-defined macropores and mesoporous skeletons via the sol–gel process accompanied by phase separation" *J. Eur. Ceram. Soc.* **2013**, *33*, 1967.
- ³⁰ X. Guo, K. Nakanishi, K. Kanamori, Y. Zhu, and H. Yang, "Preparation of macroporous cordierite monoliths via the sol–gel process accompanied by phase separation" *J. Eur. Ceram. Soc.* **2014**, *34*, 817.
- ³¹ Y. Kido, K. Nakanishi, A. Miyasaka, and K. Kanamori, "Synthesis of Monolithic Hierarchically Porous Iron-Based Xerogels from Iron(III) Salts via an Epoxide-Mediated Sol–Gel Process" *Chem. Mater.* **2012**, *24*, 2071.
- ³² C. Viklund, E. Pontén, B. Glad, K. Irgum, P. Hörstedt, and F. Svec "Molded Macroporous Poly(glycidyl methacrylate-co-trimethylolpropane trimethacrylate) Materials with Fine Controlled Porous Properties: Preparation of Monoliths Using Photoinitiated Polymerization" *Chem. Mater.* **1997**, *9*, 463.
- ³³ C. Viklund, A. Nordström, K. Irgum, F. Svec, and J. M. Fréchet, "Preparation of Porous Poly(styrene-co-divinylbenzene) Monoliths with Controlled Pore Size Distributions Initiated by Stable Free Radicals and Their Pore Surface Functionalization by Grafting" *Macromolecules* **2001**, *34*, 4361.
- ³⁴ K. Kanamori, J. Hasegawa, K. Nakanishi, and T. Hanada, "Rigid Macroporous Poly(divinylbenzene) Monoliths with a Well-Defined Bicontinuous Morphology Prepared by Living Radical Polymerization" *Adv. Mater.* **2006**, *18*, 2407.

-
- ³⁵ K. Kanamori, J. Hasegawa, K. Nakanishi, and T. Hanada, "Facile Synthesis of Macroporous Cross-Linked Methacrylate Gels by Atom Transfer Radical Polymerization" *Macromolecules* **2008**, *41*, 7168.
- ³⁶ J. Hasegawa, K. Kanamori, K. Nakanishi, T. Hanada, and S. Yamago "Pore Formation in Poly(divinylbenzene) Networks Derived from Organotellurium-Mediated Living Radical Polymerization" *Macromolecules* **2009**, *42*, 1270.
- ³⁷ R. Zhang, L. Qi, P. Xin, G. Yang, and Y. Chen, "Preparation of macroporous monolith with three dimensional bicontinuous skeleton structure by atom transfer radical polymerization for HPLC" *Polymer* **2010**, *51*, 1703.
- ³⁸ G. Hasegawa, K. Kanamori, K. Nakanishi, and T. Hanada, "Fabrication of activated carbons with well-defined macropores derived from sulfonated poly(divinylbenzene) networks" *Carbon* **2010**, *48*, 1757.
- ³⁹ J. Hasegawa, K. Kanamori, K. Nakanishi, and T. Hanada, "Macro- and microporous carbon monoliths with high surface areas pyrolyzed from poly(divinylbenzene) networks" *C. R. Chimie* **2010**, *13*, 207.
- ⁴⁰ G. Hasegawa, M. Aoki, K. Kanamori, K. Nakanishi, T. Hanada, and K. Tadanaga, "Monolithic electrode for electric double-layer capacitors based on macro/meso/microporous S-Containing activated carbon with high surface area" *J. Mater. Chem.* **2011**, *21*, 2060.
- ⁴¹ S. Peng, P. G. Hartley, T. C. Hughes, and Q. Guo, "Controlling morphology and porosity of porous siloxane membranes through water content of precursor microemulsion" *Soft Matter*. **2012**, *8*, 10493.
- ⁴² S. Yu, F. L. Ng, K. C. C. Ma, A. A. Mon, F. L. Ng, and Y. Y. Ng, "Preparation of macroporous monolith with three dimensional bicontinuous skeleton structure by atom transfer radical polymerization for HPLC" *J. Appl. Polym. Sci.* **2013**, *127*, 2641.
- ⁴³ S. Yu, K. C. C. Ma, A. A. Mon, F. L. Ng, and Y. Y. Ng, "Controlling porous properties of polymer monoliths synthesized by photoinitiated polymerization" *Polym. Int.* **2013**, *62*, 406.
- ⁴⁴ S. A. Saba, M. P. S. Mousavi, P. Bühlmann, and M. A. Hillmyer, "Hierarchically Porous Polymer Monoliths by Combining Controlled Macro- and Microphase Separation" *J. Am. Chem. Soc.* **2015**, *137*, 8896.
- ⁴⁵ N. Tsujioka, N. Hira, S. Aoki, N. Tanaka, and K. Hosoya, "A New Preparation Method for Well-Controlled 3D Skeletal Epoxy Resin-Based Polymer Monoliths" *Macromolecules* **2005**, *38*, 9901.
- ⁴⁶ A. M. Nguyen and K. Irgum, "Epoxy-Based Monoliths. A Novel Hydrophilic Separation Material for Liquid Chromatography of Biomolecules" *Chem. Mater.* **2006**, *18*, 6308.
- ⁴⁷ N. Tsujioka, N. Ishizuka, N. Tanaka, and K. Hosoya, "Well-Controlled 3D Skeletal Epoxy-Based Monoliths Obtained by Polymerization Induced Phase Separation" *J. Polym. Sci. A: Polym. Chem.* **2008**, *46*, 3272
- ⁴⁸ J. Li, Z. Du, H. Li, and C. Zhang, "Chemically Induced Phase Separation in the Preparation of Porous Epoxy Monolith" *J. Polym. Sci. B: Polym. Phys.* **2010**, *48*, 2140.
- ⁴⁹ Y. Mi, W. Zhou, Q. Li, D. Zhang, R. Zhang, G. Ma, and Z. Su, "Detailed exploration of structure formation of an epoxy-based monolith with three-dimensional bicontinuous structure" *RSC Adv.* **2015**, *5*, 55419.
- ⁵⁰ K. P. Constant, J.-R. Lee, Y.-M. Chiang, "Microstructure development in furfuryl resin-derived microporous glassy carbons" *J. Mater. Res.* **1996**, *11*, 2338–2345.
- ⁵¹ C. Liang, S. Dai, "Dual Phase Separation for Synthesis of Bimodal Meso-/Macroporous Carbon Monoliths" *Chem. Mater.* **2009**, *21*, 2115.

-
- ⁵² S. Xu, J. Li, G. Qiao, H. Wang, T. Lu "Pore structure control of mesoporous carbon monoliths derived from mixtures of phenolic resin and ethylene glycol" *Carbon* **2009**, *47*, 2103.
- ⁵³ G.-P. Hao, W.-C. Li, D. Qian, G.-H. Wang, W.-P. Zhang, T. Zhang, A.-Q. Wang, F. Schuth, H.-J. Bongard, and A.-H. Lu "Structurally Designed Synthesis of Mechanically Stable Poly(benzoxazine-co-resol)-Based Porous Carbon Monoliths and Their Application as High-Performance CO₂ Capture Sorbents" *J. Am. Chem. Soc.* **2011**, *133*, 11378.
- ⁵⁴ G. Hasegawa, Y. Ishihara, K. Kanamori, K. Miyazaki, Y. Yamada, K. Nakanishi, and T. Abe, "Facile Preparation of Monolithic LiFePO₄/Carbon Composites with Well-Defined Macropores for a Lithium-Ion Battery" *Chem. Mater.* **2011**, *23*, 5208.
- ⁵⁵ S. Xu, G. Qiao, H. Wang, D. Li, T. Lu, "Preparation of mesoporous carbon derived from mixtures of phenol-formaldehyde resin and ethylene glycol" *Mater. Lett.* **2008**, *62*, 3716.
- ⁵⁶ G. Hasegawa, K. Kanamori, and K. Nakanishi, "Facile preparation of macroporous graphitized carbon monoliths from iron-containing resorcinol-formaldehyde gels" *Mater. Lett.* **2012**, *76*, 1.
- ⁵⁷ G. Zhang, G. Liu, Z. Shi, and G. Qiao, "Dynamics of spinodal decomposition coupled with chemical reaction in thermosetting phenol-formaldehyde resin-based solutions and its application in monolithic porous materials" *RSC Adv.* **2014**, *4*, 7068.
- ⁵⁸ W. Kicinski, A. Dziura "Heteroatom-doped carbon gels from phenols and heterocyclic aldehydes: Sulfur-doped carbon xerogels" *Carbon* **2014**, *75*, 56.
- ⁵⁹ K. M. Nelson, Z.-A. Qiao, S. M. Mahurin, R. T. Mayes, C. A. Bridges, and S. Dai, "A non-micellar synthesis of mesoporous carbon via spinodal decomposition" *RSC Adv.* **2014**, *4*, 23703.
- ⁶⁰ G. Hasegawa, K. Kanamori, T. Kiyomura, H. Kurata, T. Abe, and K. Nakanishi, "Hierarchically Porous Carbon Monoliths Comprising Ordered Mesoporous Nanorod Assemblies for High-Voltage Aqueous Supercapacitors" *Chem. Mater.* **2016**, DOI: 10.1021/acs.chemmater.6b01261
- ⁶¹ D. Carriazo, M. C. Gutiérrez, M. L. Ferrer, F. del Monte, "Resorcinol-Based Deep Eutectic Solvents as Both Carbonaceous Precursors and Templating Agents in the Synthesis of Hierarchical Porous Carbon Monoliths" *Chem. Mater.* **2010**, *22*, 6146–6152.
- ⁶² M. C. Gutiérrez, D. Carriazo, C. O. Ania, J. L. Parra, M. L. Ferrer, and F. del Monte, "Deep Eutectic Solvents as Both Precursors and Structure Directing Agents in the Synthesis of Nitrogen Doped Hierarchical Carbons Highly Suitable for CO₂ Capture" *Energy Environ. Sci.* **2011**, *4*, 4201–4210.
- ⁶³ N. López-Salas, M. C. Gutiérrez, C. O. Ania, M. A. Muñoz-Márquez, M. L. Ferrer, F. del Monte, "Nitrogen-doped carbons prepared from eutectic mixtures as metal-free oxygen reduction catalysts" *J. Mater. Chem. A* **2016**, *4*, 478–488
- ⁶⁴ N. López-Salas, F. del Monte, A. Tamayo, J. L. G. Fierro, A. L. De Lacey, M. L. Ferrer, M. C. Gutiérrez, "Sulfur-Doped Carbons Prepared from Eutectic Mixtures Containing Hydroxymethylthiophene as Metal-Free Oxygen Reduction Catalysts" *ChemSusChem* **2014**, *7*, 3347–3355
- ⁶⁵ D. Carriazo, M. C. Gutiérrez, F. Picó, J. M. Rojo, J. L. G. Fierro, M. L. Ferrer, F. del Monte, "Phosphate-functionalized carbon monoliths from deep eutectic solvents and their use as monolithic electrodes in supercapacitors" *ChemSusChem* **2012**, *5*, 1405–1409.

-
- ⁶⁶ A. P. Abbott, G. Capper, D. L. Davies, R. K. Rasheed, V. Tambyrajah, "Novel solvent properties of choline chloride/urea mixtures." *Chem. Commun.* **2003**, 70–71.
- ⁶⁷ G. Imperato, E. Eibler, J. Niedermaier, B. König, "Low-melting sugar–urea–salt mixtures as solvents for Diels–Alder reactions." *Chem. Commun.* **2005**, 1170–1172.
- ⁶⁸ M. Francisco, A. van den Bruinhorst, M. C. Kroon, "Low-Transition-Temperature Mixtures (LTTMs): A New Generation of Designer Solvents." *Angew. Chem.* **2013**, 52, 3074–3085.
- ⁶⁹ M.C. Gutiérrez, D. Carriazo, C.O. Ania, J.B. Parra, M.L. Ferrer, F. del Monte, Deep eutectic solvents as both precursors and structure directing agents in the synthesis of nitrogen doped hierarchical carbons highly suitable for CO₂ capture, *Energy Environ. Sci.* **4** (9) (2011) 3535.
- ⁷⁰ N. Lopez-Salas, M.C. Gutiérrez, C.O. Ania, M.A. Muñoz-Márquez, M.L. Ferrer, F. del Monte, Nitrogen-doped carbons prepared from eutectic mixtures as metal-free oxygen reduction catalysts, *J. Mater. Chem. A* **4** (2) (2016) 478–488.
- ⁷¹ N. López-Salas, F. del Monte, A. Tamayo, J.L.G. Fierro, A.L. De Lacey, M.L. Ferrer, M.C. Gutiérrez, Sulfur-doped carbons prepared from eutectic mixtures containing hydroxymethylthiophene as metal-free oxygen reduction catalysts, *ChemSusChem* **7** (2014) 3347–3355.
- ⁷² D. Carriazo, M.C. Gutiérrez, F. Picó, J.M. Rojo, J.L.G. Fierro, M.L. Ferrer, F. del Monte, Phosphate-functionalized carbon monoliths from deep eutectic solvents and their use as monolithic electrodes in supercapacitors, *ChemSusChem* **5** (8) (2012) 1405–1409.
- ⁷³ N. López-Salas, D. Carriazo, M. C. Gutiérrez, M. L. Ferrer, C. O. Ania, F. Rubio, A. Tamayo, J. L. G. Fierro, F. del Monte, "Tailoring the textural properties of hierarchical porous carbons using deep eutectic solvents" *J. Mater. Chem. A* **2016**, *4*, 9146–9159
- ⁷⁴ J. R. Sandercock, *Light Scattering in Solids III (Chap. 6)* in *Topics in Applied Physics* **51**. Edited by M. Cardona and G. Güntherodt (Springer, Berlin), **1982**, 186.
- ⁷⁵ J. K. Krüger, *Optical Techniques to Characterize Polymer Systems (Studies in Polymer Science)*. Edited by H. Bässler (Elsevier, Amsterdam) **1989**, *5*, 429–534.
- ⁷⁶ W. Xu, E. I. Cooper, C. A. Angell, "Ionic liquids: Ion mobilities, glass temperatures, and fragilities." *J. Phys. Chem. B* **2003**, *107*, 6170–6178.
- ⁷⁵ M. C. Gutiérrez, C. R. Mateo, M. L. Ferrer, and F. del Monte, "Freeze-Drying of Aqueous Solutions of Deep Eutectic Solvents: A Suitable Approach to Deep Eutectic Suspensions of Self-Assembled Structures" *Langmuir* **2009**, *25*, 5509–5515.
- ⁷⁶ M. C. Gutiérrez, M. L. Ferrer, L. Yuste, F. Rojo, and F. del Monte, "Bacteria Incorporation in Deep Eutectic Solvents via Freeze-Drying." *Angew. Chem.* **2010**, *49*, 2158–2162
- ⁷⁷ Y. Chen, Z. Chen, S. Xiao, and H. Liu, "A novel thermal degradation mechanism of phenol–formaldehyde type resins" *Thermochim. Acta*, 2008, **476**, 39–43.

- ⁷⁸ I. L. Moudrakovski, C. I. Ratcliffe, J. A. Ripmeester, L. Q. Wang, G. J. Exarhos, T. F. Baumann and J. H. Satcher, "Nuclear Magnetic Resonance Studies of Resorcinol-Formaldehyde Aerogels" *J. Phys. Chem. B* **2005**, *109*, 11215–11222.
 - ⁷⁹ S. Mulik, C. Sotiriou-Leventis and N. Leventis, "Time-Efficient Acid-Catalyzed Synthesis of Resorcinol-Formaldehyde Aerogels" *Chem. Mater.* **2007**, *19*, 6138–6144.
 - ⁸⁰ J. Patiño, M. C. Gutiérrez, D. Carriazo, C. O. Ania, J. L. G. Fierro, M. L. Ferrer, F. del Monte, "DES assisted synthesis of hierarchical nitrogen- doped carbon molecular sieves for selective CO₂ versus N₂ adsorption " *J. Mater. Chem. A* **2014**, *2*, 8719–8729
- [84] F. Kapteijn, J.A. Moulijn, S. Matzner, H.-P. Boehm, The development of nitrogen functionality in model chars during gasification in CO₂ and O₂, *Carbon* **37** (7) (1999) 1143e1150.
- [85] J.R. Pels, F. Kapteijn, J.A. Moulijn, Q. Zhu, K.M. Thomas, Evolution of nitrogen functionalities in carbonaceous materials during pyrolysis, *Carbon* **33** (1995) 1641e1653.
- [86] R. Li, Z. Wei, X. Gou, W. Xu, Phosphorus-doped graphene nanosheets as efficient metal-free oxygen reduction electrocatalysts, *RSC Adv.* **3** (2013) 9978e9984.
- [87] J.P. Paraknowitsch, Y. Zhang, B. Wienert, A. Thomas, Nitrogen- and phosphorus-co-doped carbons with tunable enhanced surface areas promoted by the doping additives, *Chem. Commun.* **49** (2013) 1208e1210.
- [88] M.C. Gutierrez, F. Pico, F. Rubio, J.M. Amarilla, F.J. Palomares, M.L. Ferrer, F. del Monte, J.M. Rojo, PPO15-PEO22-PPO15 block copolymer assisted synthesis of monolithic macro- and microporous carbon aerogels exhibiting high conductivity and remarkable capacitance, *J. Mater. Chem.* **19** (2009) 1236e1240.
- [89] J. Schwan, S. Ulrich, V. Batori, H. Ehrhardt, S.R.P. Silva, Raman spectroscopy on amorphous carbon films, *J. Appl. Phys.* **80** (1) (1996) 440e447.
- [90] H. Passos, D.J.P. Tavares, A.M. Ferreira, M.G. Freire, J.A.P. Coutinho, Aqueous biphasic systems composed of deep eutectic solvents ternary or quaternary systems? *ACS Sustain. Chem. Eng.* **4** (5) (2016) 2881e2886.
- [91] A. Pandey, S. Pandey, Solvatochromic probe behavior within choline chloride-based deep eutectic solvents: effect of temperature and water, *J. Phys. Chem. B* **118** (50) (2014) 14652e14661.
- [92] S. Nardecchia, M.C. Gutiérrez, M.L. Ferrer, M. Alonso, I. Lopez, J.C. Rodriguez-Cabello, F. del Monte, Phase behavior of elastin-like synthetic recombinant proteins in deep eutectic solvents, *Biomacromolecules* **13** (7) (2012) 2029e2036.
- [93] D. Shah, F.S. Mjalli, Effect of water on the thermo-physical properties of Reline: an experimental and molecular simulation based approach, *Phys. Chem. Chem. Phys.* **16** (2014) 23900e23907.
- [94] C. D'Agostino, L.F. Gladden, M.D. Mantle, A.P. Abbott, E.I. Ahmed, A.Y.M. Al-Murshedi, R.C. Harris, Molecular and ionic diffusion in aqueous deep eutectic solvent mixtures: probing inter-molecular interactions using PFG NMR, *Phys. Chem. Chem. Phys.* **17** (2015) 15297e15304.
- [95] E. Posada, N. López-Salas, R.J. Jiménez-Ribó, M.L. Ferrer, M.C. Gutiérrez, F. del Monte, Reline aqueous solutions behaving as liquid mixtures of H-bonded co-solvents: microphase segregation and formation of co-continuous structures as indicated by Brillouin and ¹H NMR spectroscopies, *Phys. Chem. Chem. Phys.* **19** (2017) 17103e17110.

-
- [96] M. Mijaković, B. Kežević, L. Zoranić, F. Sokolić, A. Asenbaum, C. Pruner, E. Wilhelm, A. Perera, Ethanol-water mixtures: ultrasonics, Brillouin scattering and molecular dynamics, *J. Mol. Liq.* 164 (1e2) (2011) 66e73.
- [97] A. Asenbaum, C. Pruner, E. Wilhelm, M. Mijaković, L. Zoranić, F. Sokolić, B. Kežević, A. Perera, Structural changes in ethanol-water mixtures: ultrasonics, Brillouin scattering and molecular dynamics studies, *Vib. Spectrosc.* 60 (2012) 102e106.
- [98] L. Lupi, L. Comez, C. Masciovecchio, A. Morresi, M. Paolantoni, P. Sassi, F. Scarponi, D. Fioretto, Hydrophobic hydration of tert-butyl alcohol studied by Brillouin light and inelastic ultraviolet scattering, *J. Chem. Phys.* 134 (5) (2011) 055104.
- [99] M. Pochylski, F. Aliotta, Z. Błaszczak, J. Gapiński, Structuring effects and hydration phenomena in poly(ethylene glycol)/water mixtures investigated by Brillouin scattering, *J. Phys. Chem. B* 110 (41) (2006) 20533e20539.
- [100] L. Comez, L. Lupi, M. Paolantoni, F. Picchio, D. Fioretto, Hydration properties of small hydrophobic molecules by Brillouin light scattering, *J. Chem. Phys.* 137 (11) (2012) 114509.
- [101] F. D'Amico, F. Bencivenga, G. Camisasca, A. Gessini, E. Principi, R. Cucini, C. Masciovecchio, Thermodynamic hydration shell behavior of Glycine, *J. Chem. Phys.* 139 (1) (2013) 015101.
- [102] F. Aliotta, R. Ponterio, G. Salvato, M. Musso, Brillouin scattering evidence of nonideal mixing in methanol/CCl₄ mixtures, *J. Phys. Chem. B* 108 (2) (2004) 732e736.
- [103] M. Pochylski, F. Aliotta, Z. Błaszczak, J. Gapiński, Structural relaxation processes in polyethylene glycol/CCl₄ solutions by Brillouin scattering, *J. Phys. Chem. B* 109 (9) (2005) 4181e4188.
- [104] M. Pochylski, F. Aliotta, Z. Błaszczak, J. Gapiński, Evidences of nonideal mixing in poly(ethylene glycol)/organic solvent mixtures by Brillouin scattering, *J. Phys. Chem. B* 110 (1) (2006) 485e493.
- [105] J. Ma, C. Guo, Y. Tang, L. Chen, P. Bahadur, H. Liu, Interaction of urea with pluronic block copolymers by ¹H NMR spectroscopy, *J. Phys. Chem. B* 111
- [106] C.M. Hebling, L.E. Thompson, K.W. Eckenroad, G.A. Manley, R.A. Fry, K.T. Mueller, T.G. Strein, D. Rovnyak, Sodium cholate aggregation and chiral recognition of the probe molecule (R,S)-1,10-Binaphthyl-2,20-Diyl hydrogen phosphate (BNDHP) observed by ¹H and ³¹P NMR spectroscopy, *Langmuir* 24 (24) (2008) 13866e13874.
- [107] J. Patiño, M.C. Gutiérrez, D. Carriazo, C.O. Ania, J.L.G. Fierro, M.L. Ferrer, F. del Monte, DES assisted synthesis of hierarchical nitrogen-doped carbon molecular sieves for selective CO₂ versus N₂ adsorption, *J. Mater. Chem. A* 2 (23) (2014) 8719e8729.
- [108] N. López-Salas, M.C. Gutiérrez, C.O. Ania, J.L.G. Fierro, M.L. Ferrer, F. del Monte, Efficient nitrogen-doping and structural control of hierarchical carbons using unconventional precursors in the form of deep eutectic solvents, *J. Mater. Chem. A* 2 (41) (2014) 17387e17399.
- [109] J. Patiño, M.C. Gutiérrez, D. Carriazo, C.O. Ania, J.L. Parra, M.L. Ferrer, F. del Monte, Deep eutectic assisted synthesis of carbon adsorbents highly suitable for low-pressure separation of CO₂/CH₄ gas mixtures, *Energy Environ. Sci.* 5 (2012) 8699e8707.
- [110] Y. Zhao, L. Zhao, K.X. Yao, Y. Yang, Q. Zhang, Y. Han, Novel porous carbon materials with ultrahigh nitrogen contents for selective CO₂ capture, *J. Mater. Chem.* 22 (37) (2012) 19726e19731.

-
- [111] Y. Zhao, X. Liu, K.X. Yao, L. Zhao, Y. Han, Superior capture of CO₂ achieved by introducing extra-framework cations into N-Doped microporous carbon, *Chem. Mater.* 24 (24) (2012) 4725e4734.
- [112] X. Fan, L. Zhang, G. Zhang, Z. Shu, J. Shi, Chitosan derived nitrogen-doped microporous carbons for high performance CO₂ capture, *Carbon* 61 (2013) 423e430.
- [113] M. Sevilla, P. Valle-Vigón, A.B. Fuertes, N-doped polypyrrole-based porous carbons for CO₂ capture, *Adv. Funct. Mater.* 21 (2011) 2781e2787.
- [114] D. Li, W.B. Li, J.S. Shi, F.W. Xin, Influence of doping nitrogen, sulfur, and phosphorus on activated carbons for gas adsorption of H₂, CH₄ and CO₂, *RSC Adv.* 6 (2016) 50138e50143.
- [115] A. Sánchez-Sánchez, F. Suárez-García, A. Martínez-Alonso, J.M.D. Tascón, Influence of porous texture and surface chemistry on the CO₂ adsorption capacity of porous carbons: acidic and basic site interactions, *ACS Appl. Mater. Inter* 6 (2014) 21237e21247.